MOLECULAR
METABOLISM

Ataxin-10 is part of a cachexokine cocktail triggering cardiac metabolic dysfunction in cancer cachexia

CrossMark

Michaela Schäfer [1,2,4,13], Christian U. Oeing [3,4,14], Maria Rohm [1,2,13], Ezgi Baysal-Temel [3,4,14], Lorenz H. Lehmann [3,4,14], Ralf Bauer [3,4], H. Christian Volz [7,4], Michael Boutros [7,4], Daniela Sohn [1,2,13], Carsten Sticht [5], Norbert Gretz [5], Katrin Eichelbaum [12], Tessa Werner [10,11], Marc N. Hirt [10,11], Thomas Eschenhagen [10,11], Karin Müller-Decker [8], Oliver Strobel [9], Thilo Hackert [9], Jeroen Krijgsveld [6], Hugo A. Katus [3,4], Mauricio Berriel Diaz [1,2,13], Johannes Backs [3,4,14,**], Stephan Herzig [1,2,4,13,*]

ABSTRACT

Objectives: Cancer cachexia affects the majority of tumor patients and significantly contributes to high mortality rates in these subjects. Despite its clinical importance, the identity of tumor-borne signals and their impact on specific peripheral organ systems, particularly the heart, remain mostly unknown.

Methods and results: By combining differential colon cancer cell secretome profiling with large-scale cardiomyocyte phenotyping, we identified a signature panel of seven "cachexokines", including Bridging integrator 1, Syntaxin 7, Multiple inositol-polyphosphate phosphatase 1, Glucosidase alpha acid, Chemokine ligand 2, Adamts like 4, and Ataxin-10, which were both sufficient and necessary to trigger cardiac atrophy and aberrant fatty acid metabolism in cardiomyocytes. As a prototypical example, engineered secretion of Ataxin-10 from non-cachexia-inducing cells was sufficient to induce cachexia phenotypes in cardiomyocytes, correlating with elevated Ataxin-10 serum levels in murine and human cancer cachexia models.

Conclusions: As Ataxin-10 serum levels were also found to be elevated in human cachectic cancer patients, the identification of Ataxin-10 as part of a cachexokine cocktail now provides a rational approach towards personalized predictive, diagnostic and therapeutic measures in cancer cachexia.

1. INTRODUCTION

Cancer-induced cachexia describes a multi-factorial disease condition characterized by massive loss of adipose tissue and skeletal muscle mass and is believed to be responsible for up to 30% of cancer-related deaths in humans [1]. However, the exact causes of death and in particular the contribution of cardiac dysfunction to deaths of these patients is unclear [2]. Due to the phenotypic heterogeneity of cancer cachexia, which depends on tumor type, size and mass [3], and the mostly unknown etiology at the molecular level, cachexia still represents an immediate unmet medical need as effective and routine therapeutic measures are still lacking to date [4].

Interestingly, the clinical severity of cancer cachexia hardly correlates with tumor mass [5], indicating that the tumor controls peripheral energy balance in critical host tissues via distinct signaling mediators rather than acting as a direct "energy sink" [6]. Indeed, classical experiments demonstrated the para-biotic transfer of cachexia in rats,

[1]Institute for Diabetes and Cancer (IDC), Helmholtz Center Munich, 85764 Neuherberg, Germany [2]Joint Heidelberg-IDC Translational Diabetes Program, Inner Medicine I, Heidelberg University Hospital, 69120 Heidelberg, Germany [3]Department of Cardiology, Angiology and Pulmonology, University Hospital Heidelberg, 69120 Heidelberg, Germany [4]DZHK (German Centre for Cardiovascular Research), Partner site Heidelberg/Mannheim, 69120 Heidelberg, Germany [5]Center for Medical Research, University of Mannheim, 68167 Mannheim, Germany [6]Genome Biology Unit, EMBL, 69117 Heidelberg, Germany [7]Division of Signaling and Functional Genomics, German Cancer Research Center (DKFZ), 69120 Heidelberg, Germany [8]Core Facility Tumor Models, German Cancer Research Center (DKFZ), 69120 Heidelberg, Germany [9]Department of General Surgery, University of Heidelberg, 69120 Heidelberg, Germany [10]Department of Experimental and Clinical Pharmacology and Toxicology, University Medical Center, 20246 Hamburg-Eppendorf, Germany [11]DZHK (German Centre for Cardiovascular Research), Partner site Hamburg/Kiel/Lübeck, 20246 Hamburg-Eppendorf, Germany [12]Department for Cell Signaling and Mass Spectrometry, Max Delbrück Center, 13092 Berlin, Germany [13]German Center for Diabetes Research (DZD), 85764 Neuherberg, Germany [14]Department of Molecular Cardiology and Epigenetics, University Hospital Heidelberg, 69120 Heidelberg, Germany

*Corresponding author. Institute for Diabetes and Cancer (IDC), Helmholtz Center Munich, 85764 Neuherberg, Germany. Tel.: +49 (0)89 3187 1046. E-mail: stephan.herzig@helmholtz-muenchen.de (S. Herzig).

**Corresponding author. Department of Cardiology, Angiology and Pulmonology, University Hospital Heidelberg, 69120 Heidelberg, Germany. Tel.: +49 6221 5637714; fax: +49 6221 565573. E-mail: johannes.backs@med.uni-heidelberg.de (J. Backs).

Received October 29, 2015 • Revision received November 11, 2015 • Accepted November 18, 2015 • Available online 26 November 2015

http://dx.doi.org/10.1016/j.molmet.2015.11.004

indicating that circulating factors, rather than local tumor effects, act as causative factors in energy wasting [7].

Since the discovery of tumor necrosis factor (TNF) alpha as the wasting-associated "cachectin" [8], numerous cytokines have been discussed as pro-cachectic mediators, most notably Interleukin (IL) 6 [9]. In addition, zinc-alpha-2-glycoprotein (ZAG), also known as LMF (lipid mobilizing factor), has been identified as an adipokine with direct lipolytic action in white adipose tissue during murine and human cancer cachexia [10]. However, attempts to overcome cachectic energy wasting by therapeutically targeting these pathways remained rather disappointing and/or not feasible [11]. For example, administration of anti-TNF alpha antibodies [12] did not promote weight stabilization in human clinical trials, overall suggesting that the cancer cachectic phenotype results either from the combinatorial action of various factors or from yet to be discovered, individually acting, tumor-borne mediators. Indeed, technological limitations in both appropriate read-out systems as well as specific tumor secretome detection methods have thus far prevented the rational identification of tumor-borne signals and hampered major progress in prognostic/diagnostic/therapeutic options in cancer cachexia. Whereas the vast majority of previous studies have focused on the loss of skeletal muscle and adipose tissue as phenotypic features of cancer cachexia, recent studies suggest that other organs, i.e. the liver [13,14] and the heart [15], also play a prominent role in systemic cachexia. Indeed, cardiac failure is responsible for a substantial proportion of cancer cachexia-induced deaths [16], and classical clinical studies by Burch and colleagues already documented the presence of atrophic hearts and impairment in cardiac function in cachectic tumor patients [17]. In this respect, cancer-induced cachexia in mice was found to disrupt myocardial structure and re-activate the fetal gene program [18,19], correlating with hypo-innervation in the left ventricle [20], overall suggesting that cardiac dysfunction may represent an understudied component of systemic cancer cachexia.

Here we develop and apply cellular high throughput cardiomyocyte phenotyping to test for the cachexia-inducing capacities of a newly defined set of tumor-borne signaling mediators. These cachexokines were found to be both necessary and sufficient to trigger cardiac atrophy and metabolic dysfunction in cardiomyocytes. As a prototype, Ataxin-10 was found to be sufficient to cause cachectic cardiac phenotypes and to signal the existence of cachexia by its serum levels in murine and human model systems as well as in pancreatic cancer patients.

2. METHODS

2.1. Chemicals
All chemicals were purchased from Sigma Aldrich (Munich, Germany) unless stated otherwise. Cell culture media and supplements were from Life Technologies (Darmstadt, Germany) unless stated otherwise. Cell culture plastic ware was obtained from BD (Heidelberg, Germany) unless stated otherwise.

2.2. Animal experiments and treatments
Ectopic mouse model: 9—10 week old male Balb/c, C57BL6/N and Fox Chase SCID mice were obtained from Charles River Laboratories (CRL, Brussels, BE). Mice were injected subcutaneously into the right flank with 1.5×10^6 C26 colon carcinoma cells, 5×10^5 MC38 colon carcinoma cells and 5×10^6 SW480 cells, respectively. C26 mouse experiment: Mice were monitored for 21 days after tumor cell implantation and a cohort of mice (6 control and 10 tumor-bearing mice) was sacrificed every week after Pressure-Volume loop measurement. Echocardiography and Pressure-Volume loop (PV loop) measurement were performed weekly to assess the cardiac performance. Body composition was

determined by Echo Magnetic Resonance Imaging (EchoMRI; Echo Medical Systems, Houston, TX, USA) analysis once a week. Body weight and food intake were determined in regular intervals. MC38 mouse experiment: Mice were monitored for 30 days after tumor cell inoculation. Cardiac function was assessed by weekly echocardiography. Body composition was also measured once a week. Body weight and food intake were determined in regular intervals. SW480 mouse experiment: Mice were monitored until the onset of cachexia (15—21 days after tumor cell inoculation). Body weight was measured at regular intervals.

Orthotopic mouse model (PDAC): 10 week old male C57BL6/J mice were obtained from Charles River Laboratories (CRL, Brussels, BE). Anesthetized mice treated with 5 mg/kg Carprofen as analgesia were injected with 3000 cells (PDAC cell line #8024 or #8025; kind gift from Dieter Saur, TU Munich, Germany) into the pancreas. Mice were monitored until the onset of cachexia (24—26 days after tumor cell inoculation). Body composition was determined once a week. Body weight was measured in regular intervals.

Genetic mouse model (APC delta 580 mice): APC delta 580 mice on a C57BL6/N background were originally purchased from the National Cancer Institute (NCI) at Frederick (Frederick, MD, USA) and bred at the Animal Facility of the German Cancer Research Center (DKFZ; Heidelberg, Germany). Heterozygous APC delta 580 male mice and age-matched wild-type C57BL/6N mice with an age of 14 weeks were monitored until the onset of cachexia (at 4—6 months of age). Cardiac performance which was measured by echocardiography and body weight were determined in regular intervals.

Diabetic mice: 9—11 week old female ob/ob and db/db mice were obtained from Charles River Laboratories (CRL, Brussels, BE). After 1 week, mice were sacrificed in random fed state.

A detailed description of general animal handling, hemodynamic measurement techniques and histology can be found in the supplemental material. The animal care and all experimental protocols were reviewed and approved by local authorities (Regierungspräsidium Karlsruhe, Germany; G23/08; G12/06; G73/11; G178/13).

2.3. Cell culture
Cell lines were regularly tested for mycoplasma contamination by the company Multiplexion using Multiplex Cell Contamination Test (McCT) [21].

2.4. Preparation of conditioned supernatants (SN)
C26, MC38 (kind gift from C. Bourquin, Clinical Pharmacology, Munich, Germany) and HEK293A cells (ATCC, Manassas, VA, USA) were plated onto 15 cm plates and after reaching a confluency of ∼50% culture medium (DMEM high glucose, 10% FBS, 1% Pen/Strep) was changed. After 48 h, media were collected and the remaining cells were pelleted by centrifugation. For the treatment of cardiomyocytes, conditioned SN was 3:1 diluted in fresh culture medium. A detailed description of used transfection procedures can be found in the supplemental material.

2.5. Primary neonatal rat cardiomyocytes
Hearts were isolated from male and female Wistar rats at the age of 1—2 days. Heart slices were digested in 0.1% pancreatin. To reduce the amount of non-cardiomyocyte like epithelial cells and fibroblasts, cells were pre-plated on 15 cm plates. Afterward, cells were harvested, counted and finally plated on cell culture plates that were coated with 0.1% gelatin (BD, Heidelberg, Germany). Cells were cultured in DMEM high glucose supplemented with 10% FBS and 1% Pen/Strep. After 3 days of plating cells were treated with conditioned SN for 24 h. A detailed description of the high throughput analysis of cardiomyocyte size and immunofluorescence staining can be found in the supplemental material.
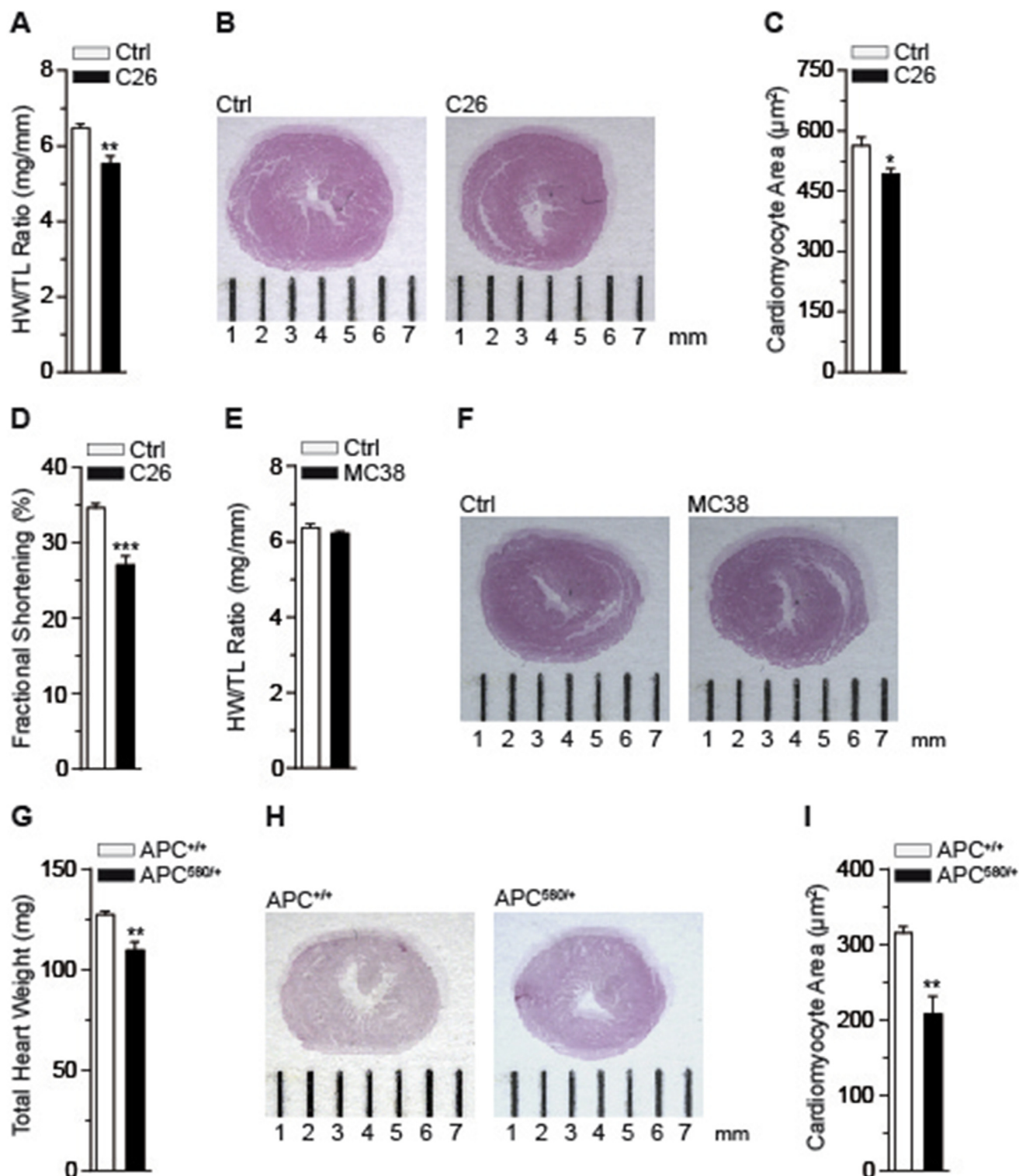
Figure 1: Cancer cachexia induces remodeling of the heart (A) Heart weight (HW)/tibia length (TL) ratio for control (Ctrl) and C26 bearing mice (C26) (n = 6 animals in Ctrl group, n = 10 animals in C26 group). **(B)** Representative overview images of H&E stained heart cross-sections of a control (Ctrl) and a C26 bearing mouse (C26). **(C)** Quantification of cardiomyocyte cross-sectional areas for control (Ctrl) and C26 bearing mice (C26) (n ≥ 100 cardiomyocytes per heart; n = 5 hearts per group). **(D)** Fractional shortening (FS) for control (Ctrl) and C26 bearing mice (C26) determined by using Vevo 2100 (n = 6 animals in Ctrl group, n = 10 animals in C26 group). **(A)−(D)** Mice were sacrificed on day 21 post PBS (Ctrl) and C26 cell injection. **(E)** Heart weight (HW)/tibia length (TL) ratio for control (Ctrl) and MC38 carrying mice (MC38) (n = 8 animals in Ctrl group, n = 10 animals in MC38 group). **(F)** Representative overview images of H&E stained heart cross-sections of a control (Ctrl) and a MC38 bearing mouse (MC38). **(G)** Total heart weight (HW) of wild-type (APC$^{+/+}$) and APC delta 580 (APC$^{580/+}$) mice (n = 6 animals in APC$^{+/+}$ group, n = 8 animals in APC$^{580/+}$ group). **(H)** Representative overview images of H&E stained heart cross-sections of a wild-type (APC$^{+/+}$) and an APC delta 580 (APC$^{580/+}$) mouse. **(I)** Quantification of cardiomyocyte cross-sectional areas of wild-type (APC$^{+/+}$) and APC delta 580 (APC$^{580/+}$) mice (n ≥ 100 cardiomyocytes per heart; n = 4 hearts per group). **(A)**, **(C)**, **(D)**, **(E)**, **(G)** and **(I)** Data are means ± SEM. *indicates significance using Student's t-test with Welch correction, *p < 0.05, **p < 0.01, ***p < 0.001.
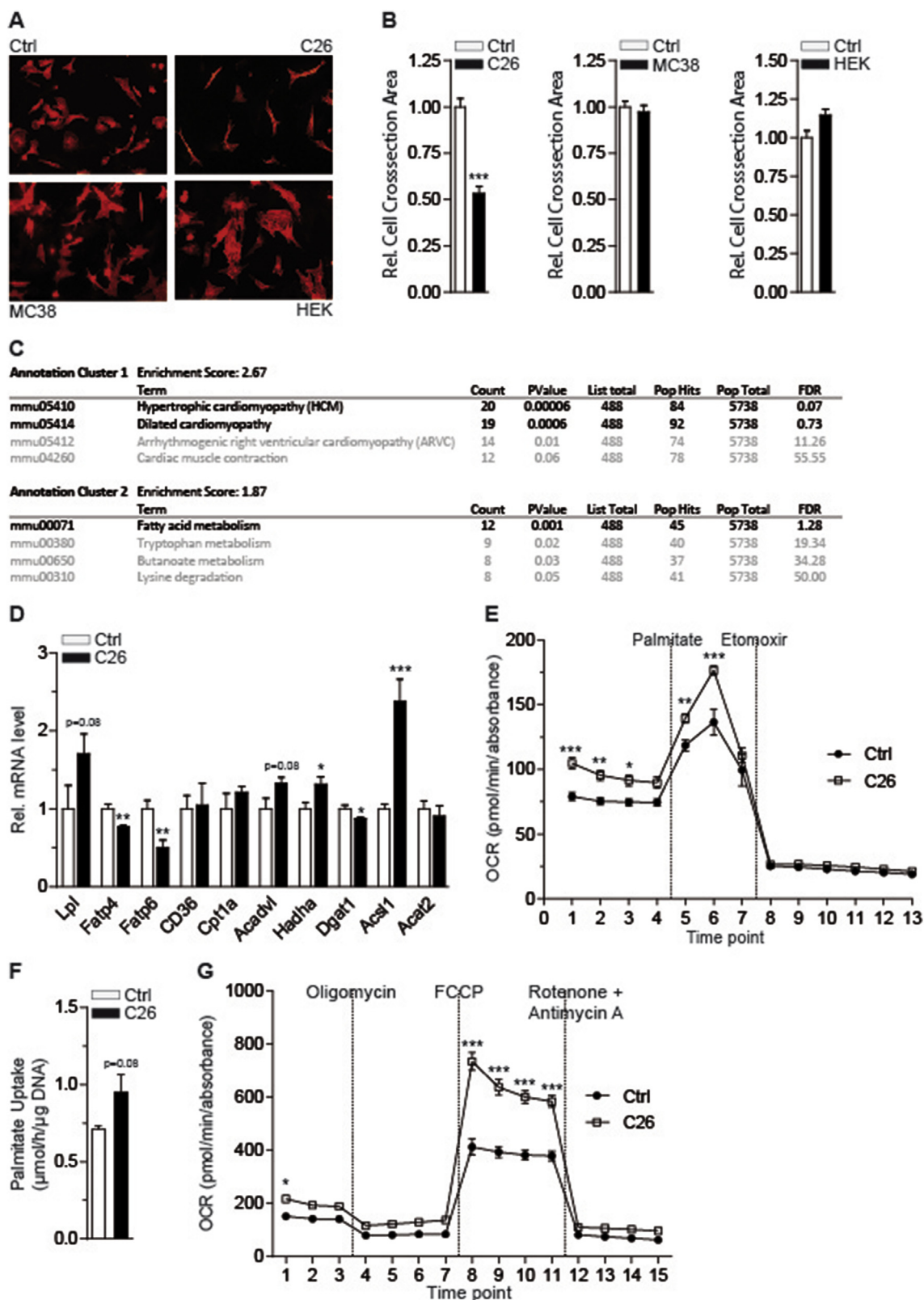
Figure 2: Tumor-borne secreted factors mediate cardiomyocyte atrophy and alter cardiomyocyte fatty acid metabolism. (A) Immunofluorescence staining of α-actinin in neonatal rat cardiomyocytes cultured in standard medium (Ctrl) or conditioned medium from C26, MC38 and HEK293A cells for 24 h, respectively (Magnification: 20×). **(B)** Relative cross-sectional areas of neonatal rat cardiomyocytes of the experiment shown in **(A)** (n ≥ 100 cardiomyocytes per condition). **(C)** Top hits (black) of KEGG pathway analysis of genes differentially regulated in primary adult mouse cardiomyocytes after treatment with conditioned medium from C26 cells for 48 h (n = 3 cell culture wells per group). **(D)** Relative mRNA level of lipoprotein lipase (Lpl), fatty acid transporter 4 (Fatp4), fatty acid transporter 6 (Fatp6), fatty acid translocase (FAT/CD36), carnitine palmitoyltransferase 1a (Cpt1a), acyl-CoA dehydrogenase, very long chain (Acadvl), hydroxyacyl-CoA dehydrogenase/3-ketoacyl-CoA thiolase/enoyl-CoA hydratase (Hadha), diglyceride acyltransferase 1

2.6. Primary adult mouse cardiomyocytes

Hearts from 9 to 10 week old anesthetized Balb/c male mice were excised and mounted on a Langendorff perfusion apparatus. A retrograde perfusion with nominally Ca^{2+}-free Tyrode's solution (pH 7.42) followed by a perfusion with digestion buffer (Tyrode's solution containing 4 mg/ml liberase 1 (Roche, Mannheim, Germany), trypsin 0.6% and 0.125 mM $CaCl_2$) was performed. After digestion, ventricular tissue was cut, dispersed, and filtered, and cells were pelleted. Cell pellet underwent a Ca^{2+} reintroduction (0.1, 0.2, 0.4 and 0.8 mM). Afterward, cell pellet was resolved in plating medium (MEM/HBSS medium containing 2 mM glutamine, 1% Pen/Strep, 10% FBS, 10 mM BDM and 2 mM Na-ATP), and cardiomyocytes were plated at 50,000 rod-shaped myocytes/well on laminin-coated 6-well plates. After 1 h, plating medium was removed and cardiomyocytes were treated with conditioned SN for 48 h. A detailed description of engineered heart tissue (EHT) and immunofluorescence staining can be found in the supplemental material.

2.7. Quantitative secretome analysis

C26 as well as MC38 cells were grown on two 10 cm cell culture dishes until they reached 60−70% confluency. Cells were cultured in SILAC medium (DMEM (non-GMP formulation w/o met, arg and lys), 10% FBS (dialyzed), 4 mM L-Glutamine, 100 mg/l Primocin) for 30 min (4 ml per dish). Subsequently, cells were incubated for 24 h in SILAC medium supplemented with 0.1 mM L-azidohomoalanine (AHA) and either 84 μg/ml [$^{13}C_6$, $^{15}N_4$] L-arginine and 146 μg/ml [$^{13}C_6$, $^{15}N_2$] L-lysine (heavy label) or 84 μg/ml [$^{13}C_6$] L-arginine and 146 μg/ml [4,4,5,5-D_4] L-lysine (intermediate label). Experiments were performed as independent biological duplicates with reversed SILAC labels. Media were collected, centrifuged, supplemented with protease inhibitor (Roche, Mannheim, Germany) and frozen at −80 °C. Enrichment of newly synthesized proteins, sample preparation for mass spectrometry, liquid chromatography tandem mass spectrometry (LC/MS), data analysis and statistics were performed as previously described [22].

2.8. Extracellular flux analysis

Neonatal rat cardiomyocytes were seeded at 5×10^4 per well onto an XF96 PS microplate (Seahorse Bioscience, Copenhagen, DK), which was coated with 0.1% gelatin. Cardiomyocytes were exposed to conditioned SN 24 h prior to the analysis. Then medium was changed to the respective assay medium. Assays were performed according to manufacturers' instructions (Seahorse Bioscience, Copenhagen, DK). Mitochondrial Stress test: Assay compounds were used at the following final concentrations: 2 μM oligomycin, 0.3 μM FCCP, 1 μM rotenone and 1 μM antimycin A. Palmitate Uptake Assay: 10 mM sodium palmitate (Sigma, #P9767) was coupled to fatty-acid free BSA (Sigma, #A8806). Both BSA-palmitate conjugate solution and beta-oxidation inhibitor etomoxir were added at a final concentration of 1 mM. Mitochondrial function assessed by oxygen consumption rate (OCR) was normalized to cell density (absorbance) determined by Sulforhodamine B staining.

2.9. Quantitative Taqman RT-PCR

Total RNA was extracted from frozen organ samples or cardiomyocytes using Qiazol reagent and RNeasy kit (Qiagen, Hilden, Germany). cDNA was prepared by reverse transcription using M-MuLV enzyme and Oligo dt primer (Thermo Scientific, Schwerte, Germany). cDNAs were amplified using assay-on-demand kits and a StepOne Real-time PCR system (Life Technologies, Darmstadt, Germany). RNA expression data were quantified according to the delta C_T method as described [23] and normalized to RNA levels of TATA-box binding protein (TBP).

2.10. Gene expression profiling

RNA isolation was performed as described before. cDNA and cRNA synthesis and hybridization to arrays of type Mouse Genome 430 2.0 from Affymetrix were performed according to the manufacturer's recommendations. A Custom CDF Version 14 with Entrez based gene definitions was used to annotate the arrays. The Raw fluorescence intensity values were normalized applying quantile normalization. Differential gene expression was analyzed based on loglinear mixed model ANOVA (Hsieh W.P., 2003; Roy J., 2007), using a commercial software package SAS® JMP7 Genomics (version 4) from SAS® (SAS® Institute, Cary, NC, USA). A false positive rate of a = 0.05 with false discovery rate (FDR) correction was taken as the level of significance. The over-representation analysis (ORA) is a microarray data analysis that uses predefined gene sets to identify a significant overrepresentation of genes in data sets [24]. Pathways belonging to various cell functions were obtained from public external databases (KEGG, http://www.genome.jp/kegg/). A Fisher's exact test was performed to detect the significantly regulated pathways. Gene Set Enrichment Analysis (GSEA) was used to determine whether defined lists (or sets) of genes exhibit a statistically significant bias in their distribution within a ranked gene list (http://www.broadinstitute.org/gsea/; [24]).

2.11. Enzyme-linked immunosorbent assay (ELISA)

Levels of human and murine Ataxin-10 were determined in conditioned SNs and sera using pre-coated Sandwich-ELISA (Uscn Life Science, Wuhan, CA). Assays were performed following the manufacturer's instructions. Conditioned SNs and human sera were measured undiluted and mouse serum was diluted 1:10/1:20.

2.12. Human subjects

Human serum samples and clinical data of patients with pathologically confirmed pancreatic ductal adenocarcinoma were derived from the prospective biobank and database of the European Pancreas Center (EPC), Department of General Surgery, Heidelberg University Hospital and were collected as approved by the local ethics committee.

Ataxin-10 (Atxn10) serum levels were determined in pre-surgery serum samples by using pre-coated Sandwich-ELISA (Uscn Life Science, Wuhan, CA, USA). Atxn10 serum levels were compared between control groups of patients with pancreatic ductal adenocarcinoma (PDAC) without cachexia (defined according to consensus classification from 2011 [25]), which did or did not receive neoadjuvant radio- and/or

---

(Dgat1), acyl-CoA synthetase long-chain family member 1 (Acsl1) and acetyl-CoA acetyltransferase 2 (Acat2) in neonatal rat cardiomyocytes cultured in standard medium (Ctrl) or conditioned medium from C26 cells (n = 4 cell culture wells per group). **(E)** Palmitate-driven oxidation of neonatal rat cardiomyocytes cultured in standard medium (Ctrl) or C26 conditioned medium for 24 h (n = 9 cell culture wells for Ctrl group, n = 15 cell culture wells for C26 group). Mitochondrial function is expressed by oxygen consumption rate (OCR; means ± SEM). 1 mM BSA-conjugated palmitate and 1 mM etomoxir were added at the indicated time points. **(F)** Uptake of ^{3}H labeled palmitate by neonatal rat cardiomyocytes cultured in standard medium (Ctrl) or C26 conditioned medium (C26) for 24 h (n = 6 cell culture wells per group). **(G)** MitoStress testing of neonatal rat cardiomyocytes cultured in standard medium (Ctrl) or C26 conditioned medium (C26) for 24 h (n = 10 cell culture wells for Ctrl group, n = 15 cell culture wells for C26 group). Mitochondrial function is expressed by oxygen consumption rate (OCR; means ± SEM). 2 μM oligomycin, 0.3 μM FCCP and 1 μM rotenone together with 1 μM antimycin A were added at the indicated time points. **(B)**, **(D)** and **(F)** Data are means ± SEM. *indicates significance using Student's t-test with Welch correction, *$p < 0.05$, **$p < 0.01$, ***$p < 0.001$. **(E)** and **(G)** Data are means ± SEM. *indicates significance using 2-way ANOVA, Bonferroni post-test, *$p < 0.05$, **$p < 0.01$, ***$p < 0.001$.
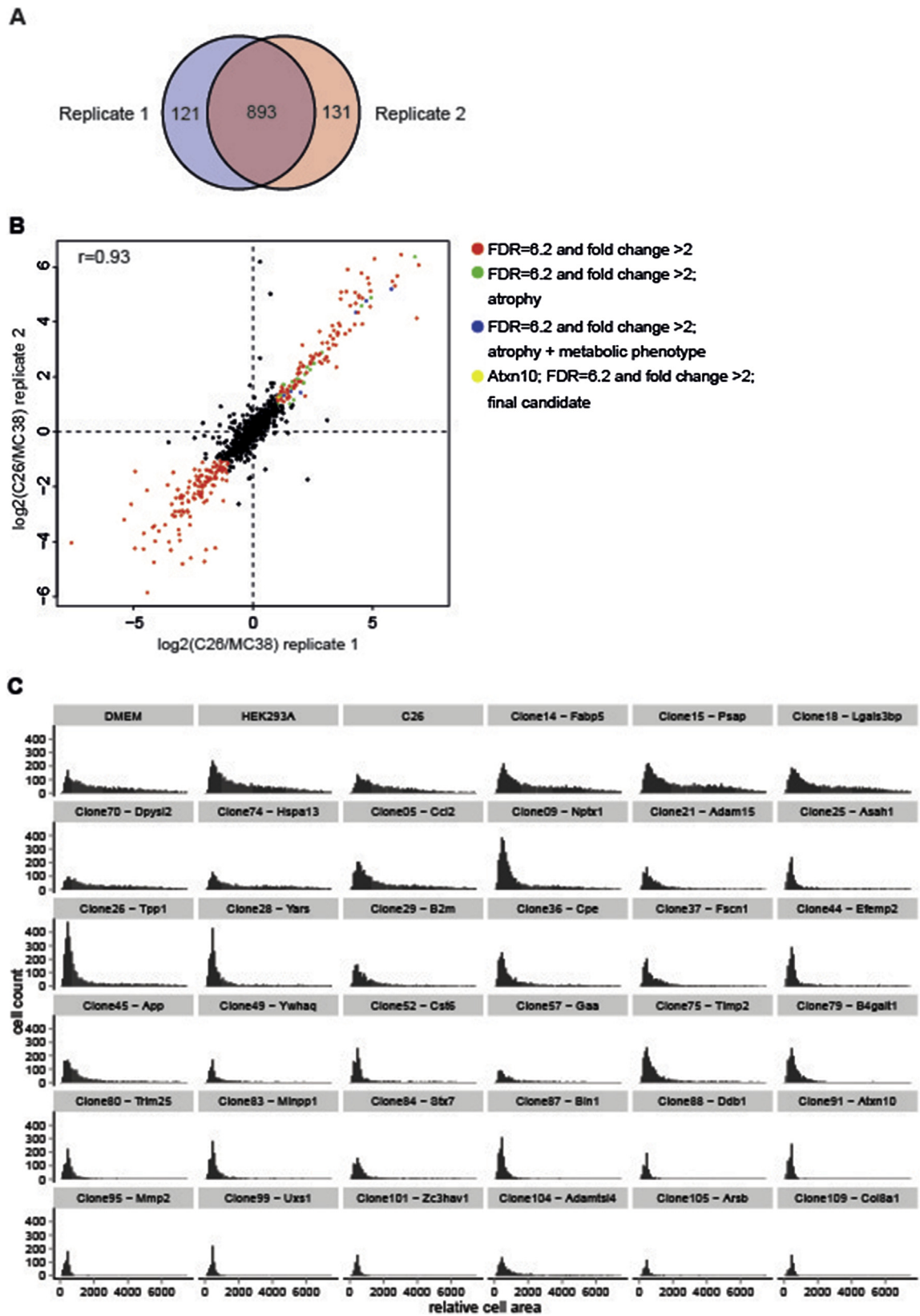
Figure 3: Quantification of pro-cachectic factors and analysis of their atrophy-inducing potential. (A) and **(B)** Quantification of secreted proteins comparing cachexia-inducing C26 cells and non-cachexia-inducing MC38 cells. **(A)** Number and overlap of proteins quantified in the two biological replicates. **(B)** Pearson correlation between the two biological replicates is 0.93. 271 of 893 proteins quantified in both replicates show significant differences between the two cell lines (red). 28 of the 129 proteins stronger secreted by C26 cells can induce atrophy (green, blue and yellow). 7 of these additionally induce a metabolic phenotype (blue and yellow). **(C)** Histogram of the 384-well high

chemotherapy (referred to as neoTx) and groups of PDAC patients with cachexia, which did or did not receive neoTx. Clinico-pathological data include tumor characteristics, therapy and weight loss and are provided in Table 3.

2.13. Statistical analysis

For each experiment, means ± SEM were determined. Statistical analysis was performed with GraphPad Prism (Version 5.0, GraphPad Software Inc., CA, USA). Statistical analyses were performed using student's t-test (Welch's test), 1-way ANOVA or 2-way ANOVA where appropriate. Correlation was determined using Spearman correlation coefficient. $p < 0.05$ was considered statistically significant.

3. RESULTS

3.1. Distinct colon cancer cell lines exert differential impacts on cardiac dysfunction

Cardiac dysfunction has been described as a severe complication in the cachectic state as induced by different cancer entities in both experimental animals and humans, including tumors of the colon, the lung, and the pancreas [15,17].

To initially delineate the cachexia-inducing properties of distinct tumor cell models *in vivo*, we employed comparative metabolic phenotyping in mice using the well-established cachexia-inducing colon (C) 26 and non-cachexia-inducing murine colon (MC) 38 adenocarcinoma transplantation models [26,27]. Three weeks after cell transplantation, subcutaneous implantation of C26 cells into wild-type mice promoted a roughly 10% loss of body weight (Figure S1A), which was associated with loss of skeletal muscle and adipose tissue mass and decreased food intake as reported previously (Figure S1B—D) [14]. Importantly, C26 tumors triggered a significant loss of heart weight (Figure 1A) with a gross reduction in heart size (Figure 1B) and cardiomyocyte diameter (Figure 1C) as compared with healthy control littermates. Notably, while no cardiac fibrosis was evident in cachectic animals (Figure S1E—H), the observed atrophy was associated with impairment of cardiac function assessed by echocardiography (Figure 1D) and of other hemodynamic parameters as determined by pressure-volume (PV) loop measurements (Figure S2A—I).

In contrast, transplantation of MC38 colon cancer cells and subsequent tumor formation in wild-type animals had no effect on body weight and fat and skeletal muscle mass as compared to non-tumor-bearing littermates (Figure S3A—C). Also, MC38 tumor formation did not affect heart weight and size (Figure 1E,F; Figure S3D) nor cardiac function in these animals (Figure S3E), indicating that the MC38 adenocarcinoma intrinsically lacks pro-cachectic properties and functionality as compared with the C26 colon cancer model *in vivo*.

To verify our findings in the C26 model in an independent genetic model of colon cancer-induced cachexia, we employed animals carrying the adenomatous polyposis coli (APC) mutation, the most common human mutation associated with colorectal cancer [28]. APC mutant animals developed numerous intestinal lesions at 5—6 month of age [29]. Lesion appearance triggered a significant reduction in body weight, skeletal muscle and WAT mass and anemia (Figure S3F—I), thereby mimicking the observed cachectic features in the C26

transplantation model. Importantly, APC mutant cachectic animals also displayed reduced heart weight and size as well as impaired cardiac function with no signs of fibrosis (Figure 1G—I; Figure S3J—L), thus validating cardiac atrophy and dysfunction in an independent experimental setting of colon cancer.

3.2. Cardiomyocyte atrophy is induced through tumor-borne secreted factors in a cell-autonomous manner

Our results thus far suggested that cardiac atrophy represents an important read-out parameter in systemic cancer cachexia with differential responsiveness to distinct colon cancer cell types.

To test whether the cachexia-inducing effect of C26 colon cancer cells is mediated by tumor-borne factors in a cell-autonomous fashion and to exclude host-derived, secondary signals, we developed an *in vitro* cardiomyocyte phenotyping system. To this end, primary cardiomyocytes were isolated from either neonatal rats or adult wild-type mice, plated onto multi-well cell culture plates, and exposed to conditioned supernatants (SN) from colon cancer and non-tumor control cell lines. Consistent with the cardiac phenotypes *in vivo* (Figure 1), exposure of primary cardiomyocytes to C26 conditioned SN triggered a substantial reduction of cardiomyocyte size in both neonatal rat and adult mouse cardiomyocytes, respectively (Figure 2A,B; Figure S4A,B). In contrast, neither MC38 nor HEK293A non-tumor SN caused cardiomyocyte atrophy under these conditions (Figure 2A,B), suggesting that C26 colon cancer cells specifically release pro-cachectic mediators that can cause cardiac atrophy in a cell-autonomous manner. In support of this notion, exposure of cardiomyocytes to serum of C26-carrying cachectic mice provoked cellular atrophy *in vitro*, the strength of which was correlating with the progression of cachexia in the donor mice (Figure S4C).

To further define the molecular-metabolic properties of cachectic cardiomyocytes, we performed comparative, high throughput transcriptome analysis in hearts from C26 tumor-carrying animals as compared with non-tumor bearing littermates and C26 SN-exposed primary mouse cardiomyocytes as compared with control SN. Remarkably, fatty acid (FA) metabolism appeared amongst the most significantly regulated gene pathways in atrophic cardiomyocytes (Figure 2C), and several genes involved in FA transport, oxidation and storage were found to be dysregulated in response to C26 SN in primary neonatal rat cardiomyocytes as demonstrated by altered mRNA levels (Figure 2D), thus confirming the *in vivo* data (Figure S4D,E).

To explore the impact of C26 SN on cardiac FA metabolism also at the functional level, we performed metabolic flux analyses in primary neonatal rat cardiomyocytes using Seahorse technology. Consistent with a reduced lipid storage capacity in both C26 SN-exposed isolated neonatal rat cardiomyocytes (Figure S5A) and hearts from C26 transplanted animals (Figure S5B), palmitate-driven FA oxidation in cardiomyocytes was significantly elevated in response to C26 SN as compared with controls (Figure 2E), correlating with a tendency to enhance cellular FA uptake under these conditions (Figure 2F). Noteworthy, mitochondrial stress testing revealed an increased maximal respiratory capacity in cardiomyocytes exposed to C26 SN (Figure 2G). These findings supported the hypothesis that atrophic cardiomyocytes switch to an energy-wasting mode in response to pro-cachectic cancer

---

throughput screening showing the areas of neonatal rat cardiomyocytes cultured in standard medium (Ctrl), under non atrophy-inducing conditions (conditioned medium from untreated HEK293A cells and HEK293A cells + cDNA clone: 14 (Fabp5), 15 (Psap), 18 (Lgals3bp), 70 (Dpysl2) or 74 (Hspa13)) and under atrophy-inducing conditions (conditioned medium from C26 cells and HEK293A cells + cDNA Clone: 5 (Ccl2), 9 (Nptx1), 21 (Adam15), 25 (Asah1), 26 (Tpp1), 28 (Yars), 29 (B2m), 36 (Cpe), 37 (Fscn1), 44 (Efemp2), 45 (App), 49 (Ywhaq), 52 (Cst6), 57 (Gaa), 75 (Timp2), 79 (B4galt1), 80 (Trim25), 83 (Minpp1), 84 (Stx7), 87 (Bin1), 88 (Ddb1), 91 (Atxn10), 95 (Mmp2), 99 (Uxs1), 101 (Zc3hav1), 104 (Adamtsl4), 105 (Arsb) or 109 (Col8a1)). (n = 6—9 cell culture wells per condition).
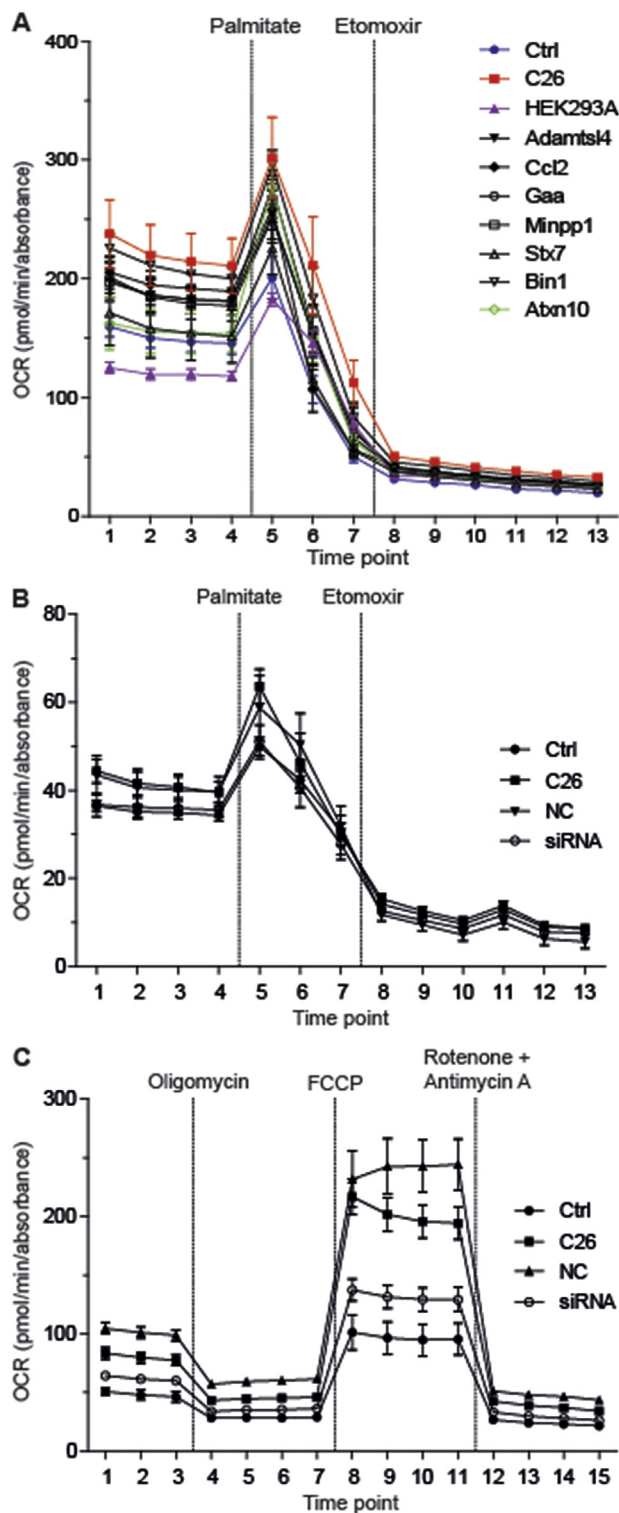
cell-derived mediators. To delineate the functional consequences of combined atrophic and metabolic changes in response to tumor cell SN, we employed engineered heart tissue (EHT) [30] in combination with enriched tumor cell SN. In congruence with a functional impairment in contractile heart function in vivo (Figure 1D; Figure S2), exposure of EHT to cachexia-inducing C26 SN diminished the contractile properties of the EHT (Figure S5C,D), thereby further substantiating the conclusion that cachexia-inducing colon cancer cells can directly impair cardiac function through secreted factors, i.e. cachexokines.

3.3. A signature of seven secreted proteins acts in a combined manner to provoke cardiac atrophy and aberrant FA oxidation

The previous experiments indicated that cachectic cardiomyocytes are characterized by two distinct features, namely reduced cell size and aberrant FA oxidation, both triggered through tumor-borne factors intrinsic to C26 but not to MC38 colon cancer cells. Indeed, heat inactivation prevented the atrophy induction by C26 SN, and withdrawal of C26 conditioned medium recovered the atrophic phenotype in cardiomyocytes (Figure S5E,F), overall suggesting that the cellular atrophy is largely conferred through protein mediators. Given the clinical importance of potential cachexokines for preventive, diagnostic and therapeutic applications, these findings prompted us to employ unbiased differential secretome analysis of C26 and MC38 tumor cells. To this end, we combined click chemistry and pulsed stable isotope amino acid labeling in both C26 and MC38 cells to selectively enrich and quantify secreted proteins from both cell lines. The combination of these two labeling approaches allows the identification of secreted proteins irrespective of the complexity of the background proteins, and thus the use of optimal growth conditions (i.e. the presence of serum) [22]. Mass-spectrometry-based identification of C26 and MC38 secretomes and differential secretome mapping established a total of 893 reproducibly secreted proteins from either C26 or MC38 cells, respectively (Figure 3A). Out of these factors, 129 proteins were found to be at least 2-fold more abundant in the C26 secretome as compared with MC38, while 142 proteins were at least 2-fold more abundant in the MC38 secretome (Figure 3B; Table 1).

We hypothesized that amongst the 129 secreted proteins with relative enrichment in cachexia-inducing C26 tumors, individual or a combination of secreted proteins would be able to impose the cardiac cachectic phenotype described above (Figure 2).

To directly test the pro-cachectic potential of identified candidates in an unbiased fashion, we obtained cDNA clones and over-expressed 109 candidates (Table 2) in non-cancerous HEK293A cells (Figure S5G). Candidate-enriched SN (Figure S5H) from these cells was collected and assayed for its atrophy-inducing potential on primary neonatal rat cardiomyocytes using a high throughput, automated 384-well screening format. In congruence with our hypothesis, SN from 28 out of 109 transfected cell clones indeed caused cardiomyocyte atrophy in repeated screening rounds (Figure 3C), and their impact on

Figure 4: Selective cachexokines provoke aberrant fatty acid metabolism in cardiomyocytes. (A) Palmitate-driven oxidation of neonatal rat cardiomyocytes cultured in standard medium (Ctrl), conditioned medium from C26 cells or HEK293A cells that were either untreated (HEK293A) or over-expressed one of the selective "cachexokines" (Adamts like 4 (Adamtsl4), Chemokine ligand 2 (Ccl2), Glucosidase alpha acid (Gaa), Multiple inositol-polyphosphate phosphatase 1 (Minpp1), Syntaxin 7 (Stx7), Bridging integrator 1 (Bin1) and Ataxin-10 (Atxn10)) for 24 h (n = 5 cell culture wells for Ctrl, C26, HEK293A, Gaa and Stx7 group, n = 6 cell culture wells for Adamtsl4, Ccl2, Minpp1, Bin1 and Atxn10 group). Mitochondrial function is expressed by oxygen consumption rate (OCR; means ± SEM). 1 mM BSA-conjugated palmitate and 1 mM etomoxir were added at the indicated time points. **(B)** Palmitate-driven oxidation of neonatal rat cardiomyocytes cultured in standard medium (Ctrl), conditioned medium from untreated C26 cells or C26 cells that were treated with either negative control (NC) siRNA or siRNAs directed against all 7 remaining candidates (siRNA) for 24 h (n = 7 cell culture wells for NC and siRNA group, n = 9 cell culture wells for Ctrl and C26 group). **(C)** MitoStress testing of neonatal rat cardiomyocytes cultured as described for **(B)** (n = 10 cell culture wells per group). Mitochondrial function is expressed by oxygen consumption rate (OCR; means ± SEM). 2 μM oligomycin, 0.3 μM FCCP and 1 μM rotenone together with 1 μM antimycin A were added at the indicated time points.
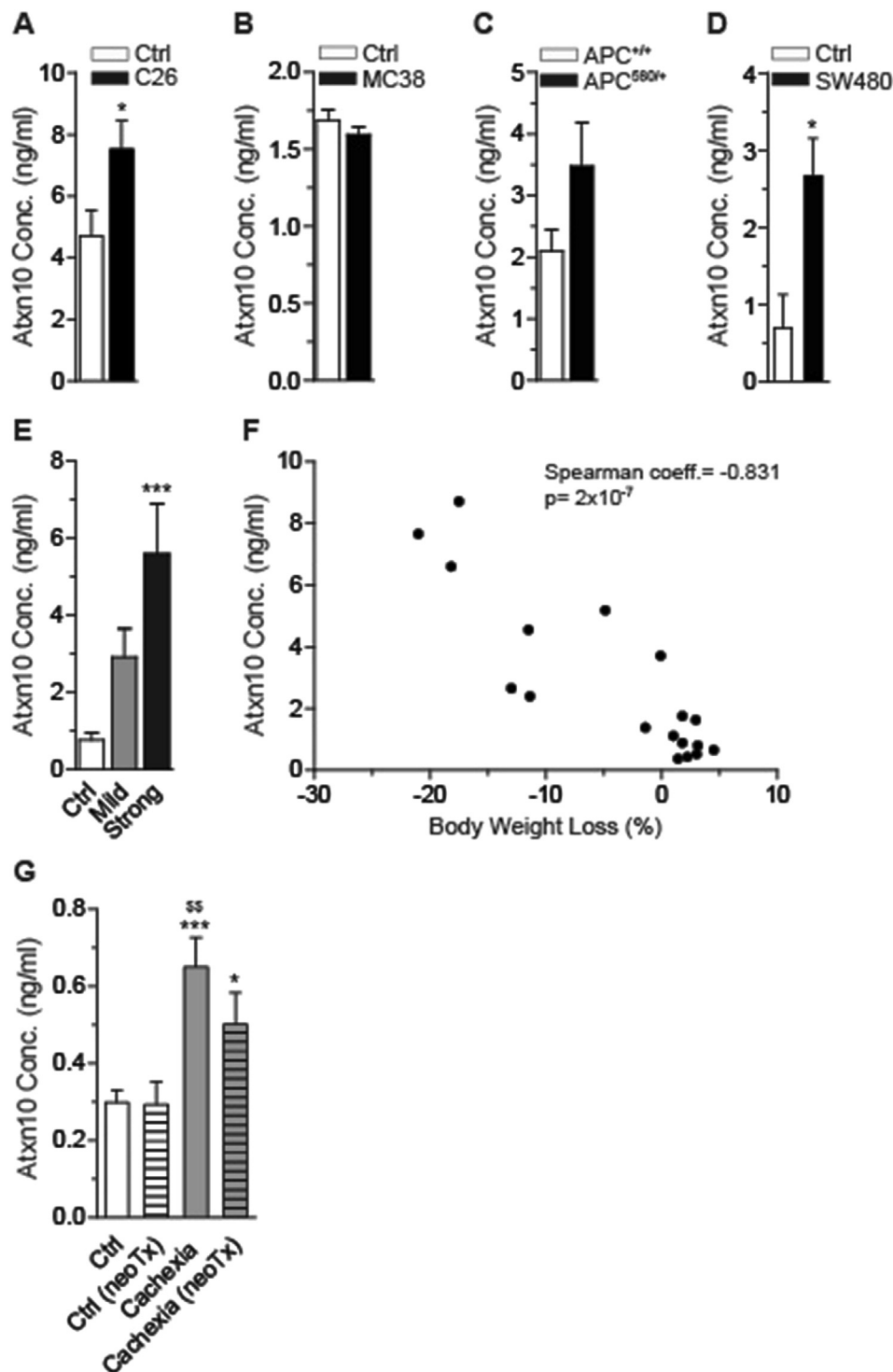
Figure 5: Serum Ataxin-10 levels are elevated under cachectic conditions. (A)−(D) Ataxin-10 (Atxn10) serum levels in different mouse models: (A) C26 (n = 6 animals in Ctrl group, n = 9 animals in C26 group), (B) MC38 (n = 3 animals in Ctrl group, n = 4 animals in MC38 group), (C) APC delta 580 (n = 5 animals in APC$^{+/+}$ group, n = 6 animals in APC$^{580/+}$ group) and (D) SW480 (n = 3 animals in Ctrl group, n = 6 animals in SW480 group). (E) Ataxin-10 (Atxn10) serum levels in wild-type mice (Ctrl) and mice with mild (mean body weight loss: 2.5%) and strong (mean body weight loss: 17%) cachectic phenotype that underwent orthotopic implantation of pancreatic cancer cells (n = 7 animals in Ctrl group, n = 6 animals in mild cachectic group, n = 5 animals in strong cachectic group). (F) Spearman correlation of Ataxin-10 (Atxn10) serum level and body weight loss (%) in the pancreatic orthotopic implantation mouse model (Coefficient (coeff.) = −0.831), p-value: 2×10^{-7}). (G) Ataxin-10 (Atxn10) serum levels in pancreatic ductal adenocarcinoma patients (PDAC) without cachexia and neoadjuvant therapy (neoTx) (Ctrl), PDAC patients without cachexia but neoTx (Ctrl (neoTx)), PDAC patients with cachexia but without neoTx (Cachexia) and PDAC patients with cachexia and neoTx (Cachexia (neoTx)) (n = 24 patients in Ctrl group, n = 8 patients in Ctrl (neoTx) group, n = 10 patients in Cachexia group, n = 10 patients in Cachexia (neoTx) group). (A)−(D) Data are means ± SEM. *indicates significance using Student's t-test with Welch correction, *p < 0.05. (E) Data are means ± SEM. *indicates significance using 1-way ANOVA, Bonferroni post-test, compared to Ctrl group, ***p < 0.001. (G) Data are means ± SEM. *indicates significance using 1-way ANOVA, Tukey's multiple comparison test, compared to Ctrl group, *p < 0.05, ***p < 0.001. $^{\$}$indicates significance using 1-way ANOVA, Tukey's multiple comparison test, compared to Ctrl (neoTx) group, $^{\$\$}$p < 0.01.

cardiomyocyte size could be validated by subsequent small-scale *in vitro* phenotyping as described above (Figure S5I). Next, the selected C26-derived secreted proteins were further filtered for their potential impact on cardiac FA oxidation as determined by metabolic flux analysis in primary neonatal rat cardiomyocytes. As shown in Figure 4A, enriched SN from 7 out of 28 *bona fide* atrophy-inducing mediators (Bridging integrator 1 (Bin1), Syntaxin 7 (Stx7), Multiple inositol-polyphosphate phosphatase 1 (Minpp1), Glucosidase alpha acid (Gaa), Chemokine ligand 2 (Ccl2), Adamts like 4 (Adamtsl4) and Ataxin-10 (Atxn10) — enhanced palmitate-driven FA oxidation, thereby mimicking the dual effect of full C26 SN in terms of cardiomyocyte size reduction and FA metabolism (Figure 4A; Figure S6A).

These experiments thus identified a signature panel of 7 cachexokines that were sufficient as individual factors to drive cardiomyocyte dysfunction in response to colon cancer growth independent from secondary host responses.

To next determine whether individual cachexokines were not only sufficient but also necessary to promote a cardiac cachectic phenotype, we employed siRNA-based knockdown strategies to silence the expression of the identified cachexokine signature panel in C26 colon cancer cells. Remarkably, SN from C26 cells depleted in individual cachexokines (Figure S6B) still promoted cellular atrophy of primary neonatal rat cardiomyocytes as compared with SN from control siRNA-transfected or parental C26 cells. In addition, individual cachexokine deficiency in C26 colon cancer cells did not improve the fatty acid metabolism phenotype, promoting the conclusion that individual cachexokines although sufficient to trigger a cardiac cancer cachectic phenotype may normally be required to act in a combinatorial fashion to confer a full cachectic response. Indeed, simultaneous ablation of all seven cachexokines in C26 colon cancer cells (Figure S6C) was able to prevent the SN-induced dysmetabolic phenotype in isolated cardiomyocytes as compared with the parental or control siRNA-transfected C26 SN (Figure 4B,C), underlining the notion that the seven cachexokines act in a combinatorial manner to specifically target cardiomyocyte function and metabolism during cancer cachexia.

3.4. Ataxin-10 correlates with weight loss in murine cachexia models and marks cachexia in cancer patients

In order to provide proof-of-concept and to test for a potential significance of a prototype cachexokine to serve as diagnostic and/or prognostic marker, we screened the serum levels of Ataxin-10, which had initially been shown to display the most robust differential secretion between C26 and MC38 colon cancer cells (Figure 3B; Table 1; Figure S7A,B) in a variety of cancer cachexia mouse models. Consistent with the pro-cachectic properties of Ataxin-10-enriched SN in cellular co-culture studies, serum levels of Ataxin-10 were elevated in C26-carrying mice and APC mutant mice but not MC38 carrying mice (Figure 5A—C), correlating with the cachectic and non-cachectic phenotype, respectively. Importantly, Ataxin-10 serum levels were also induced 4-fold in an additional independent cachexia model using human SW480 colon cancer cells in a SCID mouse background (Figure 5D). Intriguingly, tumor-induced cachexia mediated by orthotopic implantation of pancreatic cancer cells into C57BL6 wild-type mice (Figure S7C—E) led to an up to 6-fold elevation of circulating Ataxin-10 levels, which tightly correlated with the degree of body wasting (Figure 5E,F), indicating that the elevation of Ataxin-10 serum levels may serve as a prognostic/diagnostic biomarker for both murine as well as human colon cancer. Interestingly, Ataxin-10 levels were also significantly elevated in two mouse models of obesity and type 2

diabetes (Figure S7F,G), suggesting that this marker might also be indicative of cardiac dysfunction under distinct metabolic conditions that resemble the cancer cachectic phenotype [31].

To finally explore the validity of this hypothesis in humans, we determined Ataxin-10 serum levels in a cohort of cachectic and non-cachectic pancreatic cancer patients (Table 3). Of note, Ataxin-10 levels were significantly elevated in serum from cachectic patients that were untreated or received neoadjuvant radio- and/or chemotherapy (RTx, CTx) as compared to weight stable subjects that were either treated with radio- and/or chemotherapy or untreated (Figure 5G), overall demonstrating that Ataxin-10 represents a prototypical and conserved member of the cardiac-directed cachexokine signature that imposes cardiac atrophy, contractile dysfunction and aberrant lipid metabolism in cancer cachexia and may serve as a prognostic factor in human cancer cachectic patients.

4. DISCUSSION

Cancer cachexia represents a severe clinical condition for which no effective diagnostic, preventive or therapeutic measures are available to date [6]. While it has become clear that metabolic disturbances play a major role in the development of cachexia [16], and already classical experiments suggested the presence of circulating pro-cachectic factors [7], the rational identification of tumor-borne cachexokines has been hampered by technological obstacles in the past decades [6], including limitations in reliable detection methods in body fluids and the absence of relevant phenotypic read-out systems.

Our studies now provide a first unbiased and functional screening setup for the discovery of *bona fide* cachexokines with both sufficient and necessary cachexogenic properties. In this context, the established cardiomyocyte phenotyping system can potentially set the framework for an *in vitro* diagnostic tool to predict and/or diagnose pro-cachectic mediators in patient samples in a large-scale format.

Of note, the cardiomyocyte setting can be anticipated to monitor only a subset of heart-specific "cachexokines". Indeed, while the aim of our current study was to specifically screen for heart-specific cachexia signaling cues, the overall cachexokine profile from C26 cells may represent a valuable starting point to interrogate the functionality of additional factors in other tissue compartments.

In addition, it will be interesting to determine the interplay between our newly identified mediators and previously described pharmacological attempts to ameliorate tumor-induced cardiac cachexia [2], including the beta-blocker bisoprolol and the aldosterone antagonist spironolactone. Given the obvious complexity of cachexia-triggering signaling pathways, it will be interesting to determine potential points of convergence amongst these divergent pathways to pinpoint critical intracellular nodes in the cachectic cardiomyocyte.

Of note, impaired heart function is often associated with fibrosis, which results in stiffness [32], and a number of other studies reported an increase in cardiac fibrosis in the tumor-bearing situation [2,15,18]. However, in our study, neither induction of fibrosis nor a rise in appropriate markers was observed. Also, trichrome staining did not reveal an increase in collagen deposition in all animal models investigated. We speculate that the reasons for these discrepancies probably lie in the use of distinct C26 sub-clones and/or different degrees of cachexia at the time of sacrifice. In addition, recent studies have highlighted the importance of the immediate tumor environment (e.g. subcutaneous vs. intraperitoneal implantation sites) for the cachexia-inducing properties of a given tumor [33], which might also explain

seemingly contradictory observations with respect to a fibrotic phenotype. However, we did observe a change in the type of collagens, i.e. downregulation of collagen III and simultaneous upregulation of collagen I. As a higher collagen I to III ratio leads to reduced tissue function due to enhanced stiffness [34], it is tempting to speculate that the imbalance of the two collagen types promotes the observed cardiac dysfunction in our setting.

With respect to heart function, our studies indicate that alterations in fatty acid and/or lipid metabolism represent distinct features of the cachectic heart. In line with previous studies [35], it is tempting to speculate that inefficient mitochondrial FA oxidation and an increased uncoupling potential in cardiomyocytes, as previously described in cachectic skeletal muscle [36], contributes to an energy deficient state and ultimately cellular atrophy as observed by us and others [15,18]. In any case, it will be mandatory to put cachexia-associated alterations in FA oxidation into perspective with additional mechanisms contributing to cardiac dysfunction in cachexia, most notably including the induction of autophagy [15], hypo-innervation [20], and altered mTOR signaling [37]. However, while the molecular mechanisms of cachexokine-induced FA metabolic dysfunction and its relative contribution to a cachectic heart phenotype remain to be defined in future studies, it is evident that "metabolocentric" therapeutic approaches clearly have to be considered more extensively to overcome cardiac dysfunction and eventually mortality in cancer cachectic patients.

At the systemic level, most cachectic phenotypes have been ascribed to the combinatorial action of both tumor- and host-derived mediators, most notably including members of the cytokine family [38]. Our results now raise the intriguing possibility that particular tumor-borne cachexokine signatures indeed exist that are sufficient and necessary to provoke a full-blown cachectic phenotype, independent from secondary host responses. Considering that the combined but not the single knockdown of 7 potential cachexokines was sufficient to rescue the metabolic phenotype and that the combined knockdown failed to prevent the cardiac atrophy, it can be hypothesized that the overall cachectic phenotype is induced by combinatorial effects of several tumor secreted factors, influencing very distinct aspects of the overall pathology. Most clinical interventions have focused on single pro-cachectic factors known for decades, and treatments with long-term beneficial effects still do not exist. Our studies support the notion that the development of new therapeutic targets could be based on tumor-specific secretome profiles. In this respect, it is tempting to speculate about the degree of secretome overlaps between different tumor entities. Indeed, while Ataxin-10 represents a common feature of both colon and pancreatic tumor secretomes, future experimental studies will need to define the secretomes of other tumor entities to establish common or distinguishing signatures. We hypothesize that tumor-specific secretome profiling and the identification of cachectic pathways driven by specific cachexokine signatures will increase the chance to find therapeutic modalities in cancer cachectic patients, as previously exemplified by antagonism against the high affinity activin type 2 receptor ActRIIB in skeletal muscle atrophy [39,40]. These considerations should of course take into account other systemic parameters including the impact of chemotherapy as a confounding factor in many cancer cachectic patients [41].

Given the relevance of our findings also for the human setting (Figure 5), our study may pave the way for as yet unprecedented diagnostic, preventive, and therapeutic approaches in cancer cachexia, potentially using the Ataxin-10 marker as a valid starting point. Noteworthy, as all tumor-induced pathophysiological features of the heart were also described for patients with heart failure [42], one should consider adding the assessment of cardiac function to the list of diagnostic criteria for cancer cachexia. The presented data show that reduction in cardiac function occurred stepwise and already began in the pre-cachectic state which could be used for the prognostic classification of tumor patients in the future.

CONFLICT OF INTEREST

None declared.

AUTHOR CONTRIBUTIONS

M.S., E.B.-T., M.R., C.U.O., L.H.L., R.B., H.C.V., M.B., D.S., C.S., N.G., K.E., M.N.H., T.W., K.M.-D., J.K., and M.B.D. performed experiments. T.H. and O.S. supervised and coordinated patient recruitment. T.E. and H.A.K. supervised and coordinated special techniques. J.B. and S.H. designed and directed research and wrote the manuscript.

APPENDIX A. SUPPLEMENTARY DATA

Supplementary data related to this article can be found at http://dx.doi.org/10.1016/j.molmet.2015.11.004.

REFERENCES

[1] Fearon, K., Arends, J., Baracos, V., 2013. Understanding the mechanisms and treatment options in cancer cachexia. Nature Reviews Clinical Oncology 10: 90—99.

[2] Springer, J., Tschirner, A., Haghikia, A., von Haehling, S., Lal, H., Grzesiak, A., et al., 2014. Prevention of liver cancer cachexia-induced cardiac wasting and heart failure. European Heart Journal 35:932—941.

[3] Dewys, W.D., Begg, C., Lavin, P.T., Band, P.R., Bennett, J.M., Bertino, J.R., et al., 1980. Prognostic effect of weight loss prior to chemotherapy in cancer patients. Eastern Cooperative Oncology Group. American Journal of Medicine 69:491—497.

[4] Tisdale, M.J., 2002. Cachexia in cancer patients. Nature Reviews Cancer 2: 862—871.

[5] Martignoni, M.E., Kunze, P., Hildebrandt, W., Kunzli, B., Berberat, P., Giese, T., et al., 2005. Role of mononuclear cells and inflammatory cytokines in pancreatic cancer-related cachexia. Clinical Cancer Research 11: 5802—5808.

[6] Fearon, K.C., Glass, D.J., Guttridge, D.C., 2012. Cancer cachexia: mediators, signaling, and metabolic pathways. Cell Metabolism 16:153—166.

[7] Norton, J.A., Moley, J.F., Green, M.V., Carson, R.E., Morrison, S.D., 1985. Parabiotic transfer of cancer anorexia/cachexia in male rats. Cancer Research 45:5547—5552.

[8] Beutler, B., Cerami, A., 1986. Cachectin and tumour necrosis factor as two sides of the same biological coin. Nature 320:584—588.

Original article

[9] Strassmann, G., Fong, M., Kenney, J.S., Jacob, C.O., 1992. Evidence for the involvement of interleukin 6 in experimental cancer cachexia. The Journal of Clinical Investigation 89:1681—1684.

[10] Hirai, K., Hussey, H.J., Barber, M.D., Price, S.A., Tisdale, M.J., 1998. Biological evaluation of a lipid-mobilizing factor isolated from the urine of cancer patients. Cancer Research 58:2359—2365.

[11] Mantovani, G., Madeddu, C., 2009. Cancer cachexia: medical management. Support Care Cancer 18:1—9.

[12] Wiedenmann, B., Malfertheiner, P., Friess, H., Ritch, P., Arseneau, J., Mantovani, G., et al., 2008. A multicenter, phase II study of infliximab plus gemcitabine in pancreatic cancer cachexia. The Journal of Supportive Oncology 6:18—25.

[13] Berriel Diaz, M., Krones-Herzig, A., Metzger, D., Ziegler, A., Vegiopoulos, A., Klingenspor, M., et al., 2008. Nuclear receptor cofactor receptor interacting protein 140 controls hepatic triglyceride metabolism during wasting in mice. Hepatology 48:782—791.

[14] Jones, A., Friedrich, K., Rohm, M., Schafer, M., Algire, C., Kulozik, P., et al., 2013. TSC22D4 is a molecular output of hepatic wasting metabolism. EMBO Molecular Medicine 5:294—308.

[15] Cosper, P.F., Leinwand, L.A., 2011. Cancer causes cardiac atrophy and autophagy in a sexually dimorphic manner. Cancer Research 71:1710—1720.

[16] Tisdale, M.J., 2010. Are tumoral factors responsible for host tissue wasting in cancer cachexia? Future Oncology 6:503—513.

[17] Burch, G.E., Phillips, J.H., Ansari, A., 1968. The cachetic heart. A clinico-pathologic, electrocardiographic and roentgenographic entity. Diseases of the Chest 54:403—409.

[18] Tian, M., Nishijima, Y., Asp, M.L., Stout, M.B., Reiser, P.J., Belury, M.A., 2010. Cardiac alterations in cancer-induced cachexia in mice. International Journal of Oncology 37:347—353.

[19] Tian, M., Asp, M.L., Nishijima, Y., Belury, M.A., 2011. Evidence for cardiac atrophic remodeling in cancer-induced cachexia in mice. International Journal of Oncology 39:1321—1326.

[20] Muhlfeld, C., Das, S.K., Heinzel, F.R., Schmidt, A., Post, H., Schauer, S., et al., 2011. Cancer induces cardiomyocyte remodeling and hypoinnervation in the left ventricle of the mouse heart. PloS One 6:e20424.

[21] Schmitt, M., Pawlita, M., 2009. High-throughput detection and multiplex identification of cell contaminations. Nucleic Acids Research 37:e119.

[22] Eichelbaum, K., Winter, M., Diaz, M.B., Herzig, S., Krijgsveld, J., 2012. Selective enrichment of newly synthesized proteins for quantitative secretome analysis. Nature Biotechnology 30:984—990.

[23] Livak, K.J., Schmittgen, T.D., 2001. Analysis of relative gene expression data using real-time quantitative PCR and the 2(-Delta Delta C(T)) method. Methods 25:402—408.

[24] Subramanian, A., Tamayo, P., Mootha, V.K., Mukherjee, S., Ebert, B.L., Gillette, M.A., et al., 2005. Gene set enrichment analysis: a knowledge-based approach for interpreting genome-wide expression profiles. Proceedings of the National Academy of Sciences of the United States of America 102:15545—15550.

[25] Fearon, K., Strasser, F., Anker, S.D., Bosaeus, I., Bruera, E., Fainsinger, R.L., et al., 2011. Definition and classification of cancer cachexia: an international consensus. Lancet Oncology 12:489—495.

[26] Tanaka, Y., Eda, H., Tanaka, T., Udagawa, T., Ishikawa, T., Horii, I., et al., 1990. Experimental cancer cachexia induced by transplantable colon 26 adenocarcinoma in mice. Cancer Research 50:2290—2295.

[27] Rosenberg, S.A., Spiess, P., Lafreniere, R., 1986. A new approach to the adoptive immunotherapy of cancer with tumor-infiltrating lymphocytes. Science 233:1318—1321.

[28] Labianca, R., Merelli, B., 2010. Screening and diagnosis for colorectal cancer: present and future. Tumori 96:889—901.

[29] Kuraguchi, M., Wang, X.P., Bronson, R.T., Rothenberg, R., Ohene-Baah, N.Y., Lund, J.J., et al., 2006. Adenomatous polyposis coli (APC) is required for normal development of skin and thymus. PLoS Genetics 2:e146.

[30] Eschenhagen, T., Fink, C., Remmers, U., Scholz, H., Wattchow, J., Weil, J., et al., 1997. Three-dimensional reconstitution of embryonic cardiomyocytes in a collagen matrix: a new heart muscle model system. FASEB Journal: Official Publication of the Federation of American Societies for Experimental Biology 11:683—694.

[31] Lopaschuk, G.D., Ussher, J.R., Folmes, C.D., Jaswal, J.S., Stanley, W.C., 2010. Myocardial fatty acid metabolism in health and disease. Physiological Reviews 90:207—258.

[32] Conrad, C.H., Brooks, W.W., Hayes, J.A., Sen, S., Robinson, K.G., Bing, O.H., 1995. Myocardial fibrosis and stiffness with hypertrophy and heart failure in the spontaneously hypertensive rat. Circulation 91:161—170.

[33] Matsuyama, T., Ishikawa, T., Okayama, T., Oka, K., Adachi, S., Mizushima, K., et al., 2015. Tumor inoculation site affects the development of cancer cachexia and muscle wasting. International Journal of Cancer. Journal International du Cancer 137:2558—2565.

[34] Lapiere, C.M., Nusgens, B., Pierard, G.E., 1977. Interaction between collagen type I and type III in conditioning bundles organization. Connective Tissue Research 5:21—29.

[35] Busquets, S., Almendro, V., Barreiro, E., Figueras, M., Argiles, J.M., Lopez-Soriano, F.J., 2005. Activation of UCPs gene expression in skeletal muscle can be independent on both circulating fatty acids and food intake. Involvement of ROS in a model of mouse cancer cachexia. FEBS Letters 579:717—722.

[36] Tzika, A.A., Fontes-Oliveira, C.C., Shestov, A.A., Constantinou, C., Psychogios, N., Righi, V., et al., 2013. Skeletal muscle mitochondrial uncoupling in a murine cancer cachexia model. International Journal of Oncology 43:886—894.

[37] Manne, N.D., Lima, M., Enos, R.T., Wehner, P., Carson, J.A., Blough, E., 2013. Altered cardiac muscle mTOR regulation during the progression of cancer cachexia in the ApcMin/+ mouse. International Journal of Oncology 42:2134—2140.

[38] Argiles, J.M., Busquets, S., Toledo, M., Lopez-Soriano, F.J., 2009. The role of cytokines in cancer cachexia. Current Opinion in Supportive and Palliative Care 3:263—268.

[39] Zhou, X., Wang, J.L., Lu, J., Song, Y., Kwak, K.S., Jiao, Q., et al., 2010. Reversal of cancer cachexia and muscle wasting by ActRIIB antagonism leads to prolonged survival. Cell 142:531—543.

[40] Lokireddy, S., Wijesoma, I.W., Bonala, S., Wei, M., Sze, S.K., McFarlane, C., et al., 2012. Myostatin is a novel tumoral factor that induces cancer cachexia. The Biochemical Journal 446:23—36.

[41] Cramer, L., Hildebrandt, B., Kung, T., Wichmann, K., Springer, J., Doehner, W., et al., 2014. Cardiovascular function and predictors of exercise capacity in patients with colorectal cancer. Journal of the American College of Cardiology 64:1310—1319.

[42] Evangelista, L.S., Moser, D.K., Westlake, C., Pike, N., Ter-Galstanyan, A., Dracup, K., 2008. Correlates of fatigue in patients with heart failure. Progress in Cardiovascular Nursing 23:12—17.

'Corrigendum to "Ataxin-10 is part of a cachexokine cocktail triggering cardiac metabolic dysfunction in cancer cachexia" [Molecular Metabolism 5 (2) (2015) 67−78]'

Michaela Schäfer [1,2,4,13], Christian U. Oeing [3,4,14], Maria Rohm [1,2,13], Ezgi Baysal-Temel [3,4,14], Lorenz H. Lehmann [3,4,14], Ralf Bauer [3,4], H. Christian Volz [7,4], Michael Boutros [7,4], Daniela Sohn [1,2,13], Carsten Sticht [5], Norbert Gretz [5], Katrin Eichelbaum [12], Tessa Werner [10,11], Marc N. Hirt [10,11], Thomas Eschenhagen [10,11], Karin Müller-Decker [8], Oliver Strobel [9], Thilo Hackert [9], Jeroen Krijgsveld [6], Hugo A. Katus [3,4], Mauricio Berriel Diaz [1,2,13], Johannes Backs [3,4,14,**], Stephan Herzig [1,2,4,13,*]

The authors regret that the original paper was published with an error in the supplementary data (Table 1). In order to identify tumor-secreted factors that contribute to cardiac atrophy under the condition of cancer cachexia, in the original study, we performed a differential secretome analysis comparing cell conditioned media from cachexia-inducing C26 colon carcinoma cells and non-cachexia-inducing MC38 colon carcinoma cells. Secreted proteins which were at least 2-fold more abundantly secreted from C26 cells were selected for further functional validation. Functional validation was performed by overexpressing candidate proteins in HEK293A cells and collecting the candidate-enriched cell conditioned media for assaying their atrophy-inducing potential on primary neonatal rat cardiomyocytes.

In the context of subsequent studies focusing on different aspects of cancer-induced cachexia, we performed a differential transcriptomics analysis comparing RNAseq data from C26 and MC38 cells. While differential protein secretion does not necessarily need to be fully reflected by corresponding differences at the level of gene expression, we were still surprised about the lack of congruency between the corresponding regulation of gene expression and protein secretion. Surprisingly, for the overlap of genes and proteins being differentially regulated between C26 and MC38 cells (regardless of the direction of change), we found a significant negative correlation between differential gene expression and differential protein secretion (Corrigendum Figure 1A). In order to elucidate the basis of this unexpected finding,

we decided to repeat the differential secretome analysis in the same manner as it has been performed in the original study. Notably, the comparison between the secretome analyses (old vs new) revealed a remarkably strong negative correlation concerning the difference in protein secretion between C26 and MC38 cells (Corrigendum Figure 1B). Furthermore, when we then compared the new secretome analysis with the differences in the transcription between C26 and MC38 cells, there was a highly significant positive correlation (Corrigendum Figure 1C). The found consistency for the differences between the cell lines at distinct levels of regulation (transcription vs secretion) suggested that these datasets were correctly associated, in contrast to the previous comparison with the original differential secretome analysis. Taken together, these new analyses strongly indicate that in the original (old) secretome analysis, a swap in the sample allocation must have occurred, either during sample preparation, the subsequent proteomic or data analysis. Despite extensive evaluation of the respective experiment records, it was not possible to detect at which exact point in the course of the experimental work this mistake was made.

Remarkably enough, the high-throughput functional validation of 109 candidates performed in the original study (original manuscript Figure 3C), using selected candidates now considered to be more abundantly secreted from non-cachexia-inducing MC38 instead of cachexia-inducing C26 cells, still revealed a set of candidates
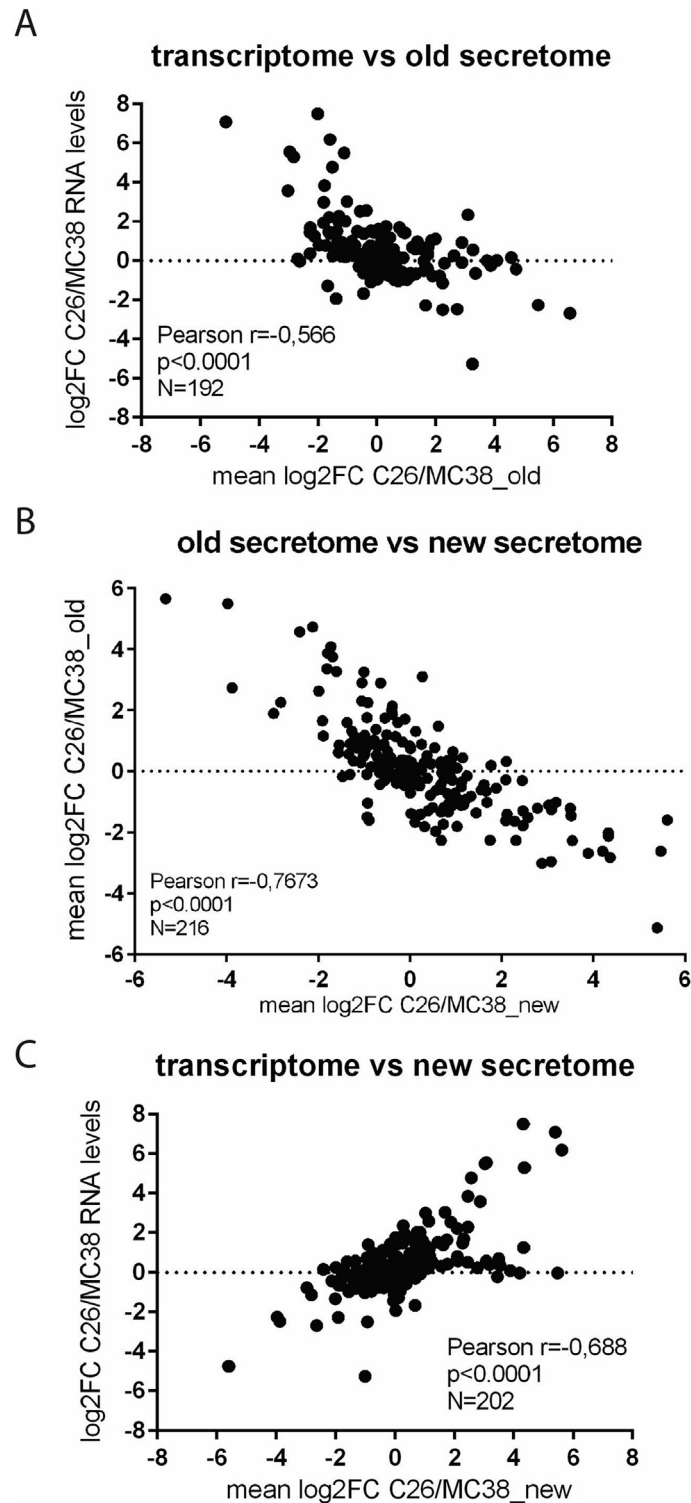
Corrigendum Figure 1: Correlation analyses of the different datasets comparing C26 and MC38 colon carcinoma cells. Correlation between (A) differentially expressed genes determined by RNAseq and the original (old) differential secretome analysis, (B) the original differential secretome analysis (old) and the new differential secretome analysis (new), (C) differentially expressed genes and the original (old) differential secretome analysis. Data are depicted as log2-fold changes (log2FC). Statistical analysis was performed by correlation analysis using Graphpad prism. N numbers, Pearson correlation coefficients (r) and statistical significance levels (p) are depicted in the graphs.

showing the expected atrophy effects upon treatment of primary cardiomyocytes with the respective candidate-enriched conditioned media. These effects were comparable to the effects of C26 conditioned medium on cardiomyocyte atrophy (original Figure 2A and B)

and were therefore applied as primary selection criterion for putative cachexokines (mediators of cachexia). Additionally, further analysis selected a subset of 7 candidates which, similar to C26 conditioned medium, increased the fatty acid oxidation rate in neonatal rat

cardiomyocytes treated with candidate-enriched medium (original Figure 4A). We speculate that the high-throughput functional analysis, albeit being based on an erroneous initial secretome analysis, contained a sufficient high number of protein candidates in order to contain protein factors which eventually turned out to be still relevant with respect to their capability to mediate a specific component of the cachexia phenotype (cardiomyocyte atrophy). This is exemplified by the main candidate Ataxin-10 (Atxn10), for which we could confirm elevated levels in different models of experimental cachexia, including C26 tumor-bearing mice but not in MC38 tumor-bearing mice (original Figure 5A—D). In a model pancreatic of cancer based on orthotopic cell implantation, circulating Atxn10 levels closely correlated with the degree of weight loss (Figure 5E and F).

Finally, we found Atxn10 levels to be elevated in cancer patients with cachexia compared to weight-stable patients (Figure 5G). Therefore, we would like to emphasize that the majority of data provided in the publication is still correct. We apologize for any inconvenience that might have resulted from providing incorrect differential secretome data as supplemental material of the study and now provide the data of the new and correct differential secretome analysis (Corrigendum supplemental data).

APPENDIX A. SUPPLEMENTARY DATA

Supplementary data to this article can be found online at https://doi.org/10.1016/j.molmet.2020.02.013.